Chain Collapse by Atomistic Simulation

Genzo Tanaka[†] and Wayne L. Mattice*

The BFGoodrich Company, 9921 Brecksville Road, Brecksville, Ohio 44141, and Maurice Morton Institute of Polymer Science, The University of Akron, Akron, Ohio 44325-3909

Received September 14, 1994; Revised Manuscript Received October 29, 1994[⊗]

ABSTRACT: In order to study the collapse of polymer chains, atomistic simulations of atactic poly(vinyl chloride) (PVC) were performed. An isolated PVC chain with a degree of polymerization (DP) larger than 40 quickly folds from an all-*trans* zigzag form into a nearly spherical compact state, whose density is close to the bulk one. PVC chains with DP < 30 remain unperturbed. The radius of gyration (S) and the monomer clustering exhibit two-stage and three-stage processes for the chain collapse, respectively. In the first stage, nearest monomers stick together and both the end-to-end distance and S sharply decrease. The shape of the chain changes from a thin wire to a sausage. The second stage corresponds to the transition from a sharp to gradual decrease in S. During this stage, distant monomers along the contour start coming within an interaction radius of each other. The third stage is characterized by an appearance of self-entanglements. In the collapsed chain, no new torsion states develop but the distribution becomes richer in *gauche*[±] states than in the unperturbed chain.

Introduction

Flexible polymer chains fold into a compact form under poor solvent conditions. Stockmayer predicted[1] the collapse point, below which only the completely collapsed coil is stable. It occurs at a negative value of the excluded volume parameter,[2] indicating that polymer chains in a poor solvent may or may not collapse at a given temperature, depending on the degree of polymerization (DP). Since then, the collapse state and transition from coil to collapse have been widely investigated experimentally,[3–12] theoretically,[13–25] and computationally.[26–33] In most theoretical and computational treatments, a polymer chain is assumed to be a string of segments.

We have studied the collapse problem by atomistic simulations of isolated chains in vacuum. The concept of a polymer chain in a vacuum and with kinetic energy that specifies a temperature of 300–600 K may seem artificial. However, if essential physics of collapse is universal, the present model must contain it. Further, the vacuum has the distinct advantages of providing a poor solvent of very low viscosity, permitting large movement of the chain on the time scale accessible by molecular dynamics. This is a self-consistent model rather than a realistic one. In this model, individual atoms have partial charges, and the electrostatic interaction between two atoms can be attractive or repulsive depending on the signs of their partial charges. The van der Waals interactions between nonbonded atoms are strongly repulsive in the short range and weakly attractive in the long range. Therefore, before the simulation it was not clear that all polymer chains collapse in vacuum. Particularly, Lee and Mattice implicitly assumed[34] that an isolated short chain in vacuum is in the unperturbed state in their calculation for the characteristic ratio of poly(vinyl chloride) (PVC) chains. We varied the DP in order to see the chain length effect on collapse. Our simulations suggest that there is a critical length region above which the chain collapses and below which it is in the unperturbed state.

* To whom correspondence should be addressed at the Maurice Morton Institute of Polymer Science.

[†] Present address: Maurice Morton Institute of Polymer Science, The University of Akron, Akron, OH 44325-3909.

[⊗] Abstract published in *Advance ACS Abstracts,* December 15, 1994.

Table 1. Meso and Racemic Sequence Distribution of a 100-Mer PVC Parent Chain

sequence	meso (%)	racemic (%)
diad	43.4	56.5
triad	17.3	30.6
tetrad	4.1	15.4
pentad	1.0	7.2

A simple decrease in chain dimensions is theoretically predicted and experimentally observed. Now we may ask whether any new torsion states are developed or only the distribution of the torsion states is shifted in the collapsed state. Further, de Gennes predicted[19] that the shape of the polymer chain varies from a coil to a sausage and to a compact sphere, and Grosberg et al. proposed[22] that the chain first forms an unknotted crumpled globule and then slowly becomes a knotted compact globule. The above two-stage kinetics was recently observed by Chu et al.[12] However, the shape and knots of the polymer chain have not been studied, since there is no direct method to experimentally observe them.

We attempt to answer the above questions by atomistic molecular modeling simulations which provide microscopic properties as well as global ones. Therefore, in the present work, we analyze conformational properties of collapsing chains such as the dimension, shape, number and distribution of neighbors, and torsion angles.

Methods and Procedures

The SYBYL molecular modeling software (Tripos Associates, Inc.) was used in this work for building polymer structures, performing energy minimization and molecular dynamics simulations, and analyzing results.

We built a 100-mer PVC chain with 56.5% racemic diads in an all-*trans* backbone conformation. The content of racemic diads is close to that of commercial PVC resins. In Table 1, fractions of meso and racemic sequences are listed. No meso and racemic sequences longer than pentads occurred in the 100-mer chain. Shorter chains were made by removing appropriate lengths of both ends, and longer ones by connecting images of this chain. The racemic content of these chains may not be equal to that of the parent chain.

0024-9297/95/2228-1049$09.00/0

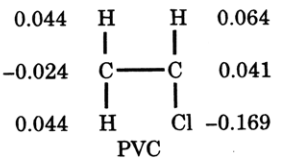

Figure 1. Partial charges for a monomeric unit of PVC determined by the Pullman method.

The potential energy function consists of harmonic bond length and bond angle 3-fold torsional 6−12 van der Waals, and Coulombic electrostatic interactions. The default values were used for the force field parameters[35] and the nonbonded cutoff distance (8 Å). The partial charges were assigned to all atoms in each chain by the Pullman method.[36] Because of the neutrality condition, atoms near both ends have slightly different values from those in the middle section. The values of the partial charges in the middle section of a chain are shown in Figure 1. The present values for PVC are quite similar to those of Ludovice and Suter[37] but considerably different from those of Smith, Jaffe, and Yoon (SJY).[38] However, SJY found electrostatic contributions to the chain dimensions of amorphous PVC systems are quite small. This suggests that in dense systems like collapsed and amorphous states, the difference in partial charges has a minor effect on chain dimensions. Therefore, we never attempted to modify the Pullman values.

The potential energy of the initial structure was minimized until the root-mean-square gradient became less than 0.08 kcal mol^{-1} Å^{-1}. After the minimization the chains remained essentially in the all-*trans* conformation.

Molecular dynamics (MD) simulations were carried out on an SGI440/GTX workstation at 300 and 600 K for 200 ps with a time step of 0.001 ps, except for 300-mer PVC which was simulated for only 150 ps.

Results and Discussion

Trajectories of Chain Dimensions. Snapshots and trajectories of the end-to-end distance (R) and the radius of gyration (S) are shown in Figure 2a−c for MD simulations of a PVC chain with 56.5% racemic diads at 300 and 600 K. The snapshots display only backbone carbon atoms. Two gray scales distinguish the middle third of each chain from the remainder. Both R and S fluctuate more at 600 K than at 300 K, and the chain folds more quickly at 600 K than at 300 K.

The trajectories may be divided into three stages depending on the profile of S:

(I_S) Sharp decrease in S and R: Both decrease nearly linearly with time. During that interval, the chain dimensions become slightly smaller than those of the unperturbed chain. Both R and S become the corresponding unperturbed values, denoted by R_0 and S_0 in Figure 2, at nearly the same time.

(II_S) Gradual decrease in S: R exhibits a local maximum.

(III_S) Nearly constant S: R fluctuates significantly.

As snapshots clearly show, stages I_S and II_S represent the transition from a fully extended conformation to a collapsed state, while stage III_S is considered as fluctuations in an equilibrium collapsed state.

The time intervals for the three stages are identified as 0−50, 50−120, and 120−200 ps for the 100-mer at 300 K, 0−30, 30−60, and 60−200 ps for the 100-mer at 600 K, and 0−50, 50−80, and 80−150 ps for the 300-mer at 600 K, respectively. In later discussion, the time-average values are taken over the third stage.

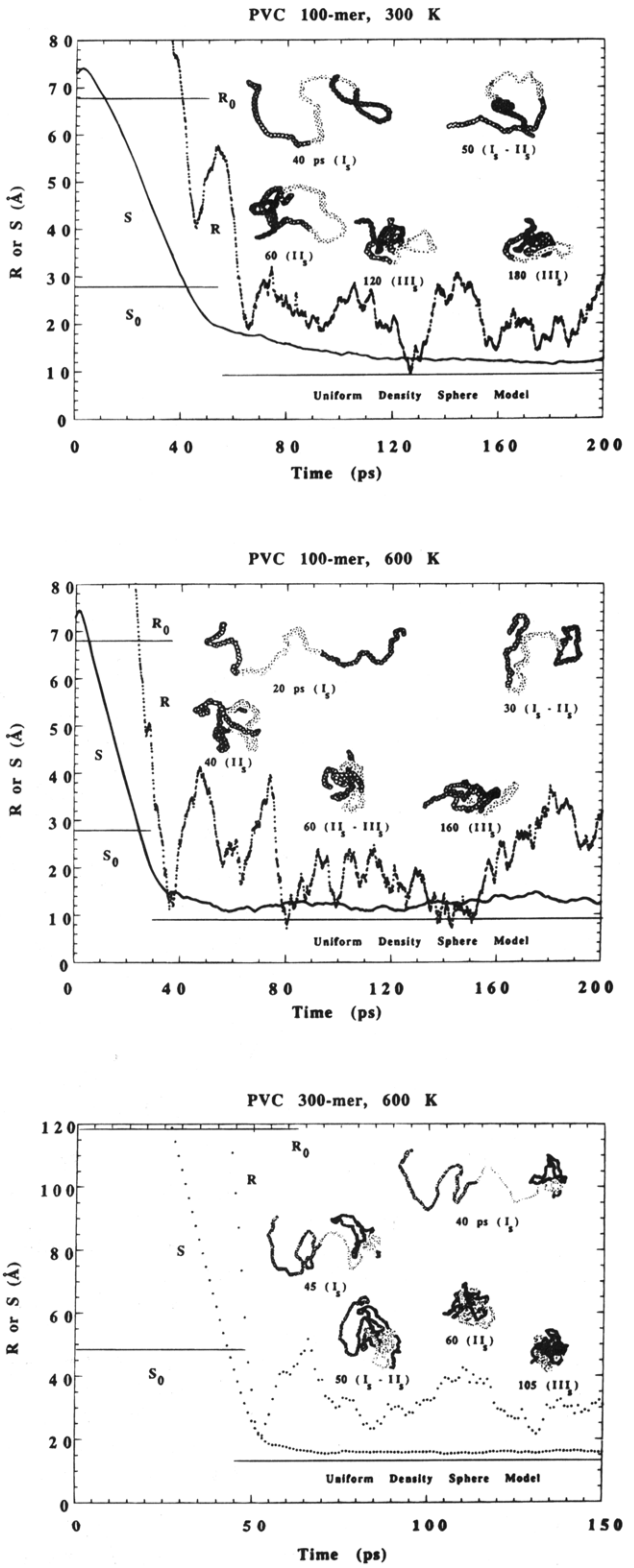

Figure 2. Snapshots and trajectories of the end-to-end distance (R) and the radius of gyration (S) for 150−200 ps MD simulations of a PVC chain with 56.5% racemic diads: (a, top) 100-mer at 300 K; (b, middle) 100-mer at 600 K; (c, bottom) 300-mer at 600 K. The horizontal lines indicate the root-mean-square unperturbed R and S (subscript 0) and S_{dense} for the uniform density sphere model. Stages I_S, II_S, and III_S are discussed in the text.

In our three simulations, the time step for the first pronounced minimum of R roughly corresponds to the end of stage I_S.

Average S and R. Time-average values of S and R are summarized in Table 2. They are much smaller

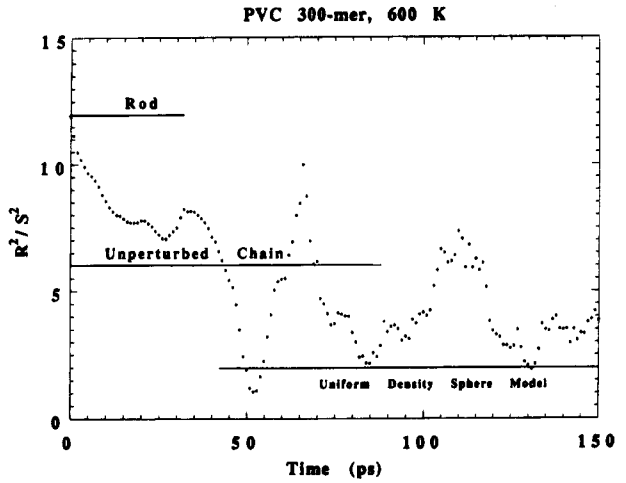

Figure 3. Variations of the squared ratio R^2/S^2 with time for the 300-mer at 600 K. Three horizontal lines represent values corresponding to the rod, unperturbed chain, and the uniform density sphere model, respectively.

Table 2. Average Dimensions (Å) and Expansion Factors for Collapsed PVC Chains

DP	T(K)	R	S	S_{min}	α_S	S_0	R_{dense}	S_{dense}	$\alpha_{S,d}$
100	300	21.1	12.8	11.3	0.46	27.8	12.1	9.4	0.34
100	600	20.0	12.4	10.7	0.45	27.8	12.1	9.4	0.34
300	600	30.9	15.9	15.3	0.33	48.2	17.4	13.5	0.28

than the root-mean-square unperturbed dimensions. In fact, the linear expansion factor α_s (=S/S_0) is 0.45−0.46 for the 100-mer and 0.33 for the 300-mer, respectively, using the characteristic ratio of 9.8[34] and assuming the square radius of gyration at the unperturbed state is one-sixth of the square end-to-end distance, $\langle S^2\rangle_0 = \langle R^2\rangle_0/6$, with subscript 0 denoting the unperturbed state.

The fluctuations of S in the completely collapsed state (stage III_S) are small. Minimum values of the radius of gyration during the simulations, S_{min}, are also listed in Table 2. The corresponding α_s are 0.38−0.41 for the 100-mer and 0.31 for the 300-mer, respectively. If all the monomers of an entire chain are uniformly distributed in a sphere of radius R_{dense} and its density is equal to the experimental density (1.4 g/cm^3 for PVC), R_{dense} and the corresponding radius of gyration, S_{dense}, are 12.1 and 9.4 Å for the 100-mer and 17.4 and 13.5 Å for the 300-mer chains, respectively. Therefore, the time-average S is 17−36% larger and S_{min} is 13−20% larger than the uniform density value, respectively. S_{dense} is shown by a horizontal line in Figure 2. Values of $\alpha_{S,d}$ corresponding to S_{dense} are also included in Table 2 as well as those of S_{dense}.

Correlation between S and R. The ratio R^2/S^2 fluctuates considerably even in stage III_S, as shown in Figure 3 for the chain with DP = 300, reflecting mainly the variation of the instantaneous R. Most values of R^2/S^2 in stage III_S are smaller than the unperturbed value of 6. It is, however, usually larger than 2, which is the expectation for the uniform density sphere model with a random location of the ends within it. Qualitatively similar behavior is observed with the chain of DP = 100.

Although it is interesting to compare their ensemble averages starting from the same initial structure with various different paths to collapse, such a task is impractical at the current level of computer capability. Instead, we approximate an ensemble average as an average over a short time interval and calculate the following correlation:

$$\varrho = \frac{\overline{R^2S^2} - 1}{\left[\left(\overline{\frac{R^4}{(R^2)^2}} - 1\right)\left(\overline{\frac{S^4}{(S^2)^2}} - 1\right)\right]^{1/2}} \qquad (1)$$

where the overlines denote the time average within the time interval chosen. It is desirable to make the time interval long to collect as many data as possible. However, a large dimensional change in the first stage (I_S) makes such an average meaningless if the interval is too long. Here, the averages were taken for a 10 ps interval. Figure 4 shows the correlation for 100-mer and 300-mer. For reference purposes, $\varrho_R = \overline{R^4}/\overline{(R^2)^2} - 1$, $\varrho_S = \overline{S^4}/\overline{(S^2)^2} - 1$, and $\varrho_{RS} = \overline{R^2S^2}/\overline{(R^2)}\,\overline{(S^2)} - 1$ are also included. The unperturbed value for ϱ is indicated by a vertical line. It is calculated using the known even moments[2] and $\langle R^2S^2\rangle_0/\langle R^2\rangle_0\langle S^2\rangle_0 = 4/3$.[39]

$\varrho \approx 1$ during stage I_S (until 40, 35, and 50 ps for 100-mer at 300 K, 100-mer at 600 K, and 300-mer at 600 K, respectively). After that, ϱ scatters. That is, R and S are strongly correlated with each other in stage I_S; however, such a correlation is quickly lost after the transition to stage II_S. The individual components, ϱ_R, ϱ_S, and ϱ_{RS}, exhibit a peak at or just before the end of stage I_S, reflecting large fluctuations in R and S. The higher the temperature and DP, the larger the fluctuations. For 300-mer chains at 600 K, all three ratios exceed the corresponding unperturbed values at 50 ps. These findings are in good agreement with a recent mean-field theory prediction.[24]

S vs Energy. A plot of the potential energy versus S is displayed in Figure 5 for eight conformations selected from the MD trajectory for the 100-mer PVC chain at 600 K and then subjected to energy minimization. Two vertical arrows indicate the values of $\langle S^2\rangle_0^{1/2}$ and S_{dense} for the uniform density sphere model calculated from the experimental density mentioned above. The potential energy (solid circles in Figure 5a) remains nearly constant for conformations where $S > 0.75S_0$. For more compact conformations, it sharply decreases as S approaches S_{dense}. This behavior demonstrates that the isolated PVC chain is energetically stable in a tightly coiled state.

The total potential energy is decomposed into seven components, and they are also shown in Figure 5 as a function of S. The bond length energy remains constant while bond angle and torsion contributions tend to increase as the chain collapses. These covalent components are always positive. The nonbonded interactions are divided into the 1−4 term and the rest.

The 1−4 component of the van der Waals energy is positive at the beginning, drops to a small negative value, and gradually returns to a positive one. Both electrostatic terms are nearly constant but their effects are opposite. Its 1−4 component is strongly attractive and the other component is moderately repulsive. The net electrostatic interactions are attractive and remain constant. The long-range van der Waals component is slightly positive for extended chains but soon becomes negative and sharply decreases as S approaches S_{dense}. This term is responsible for the collapse of the PVC chain. The electrostatic interactions turn out to be insignificant for the collapse of the PVC chains.

The difference in potential energy between the collapsed and loose coil is about 150 kcal mol^{-1} or 1.5 kcal

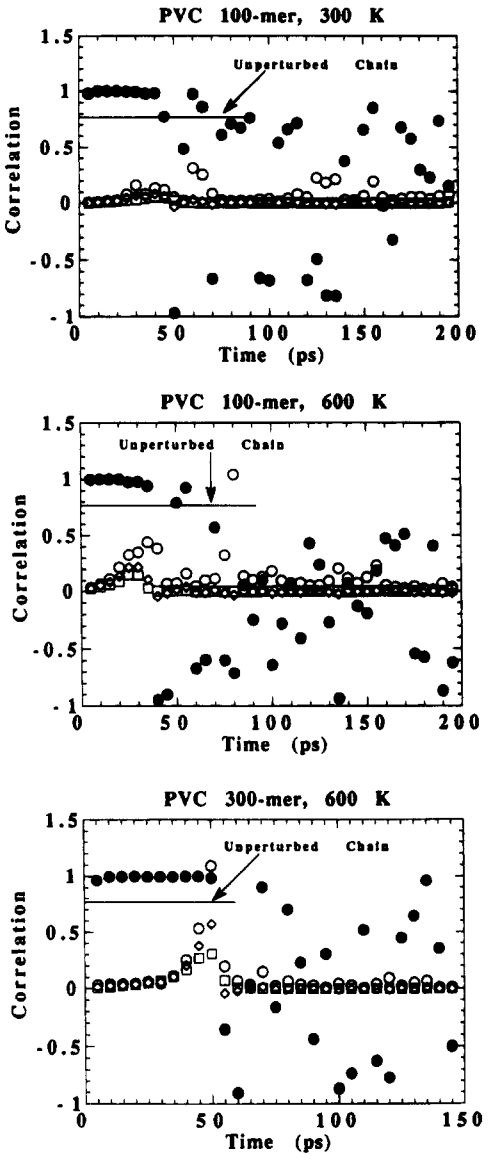

Figure 4. Correlation between the square end-to-end distance (R^2) and square radius of gyration (S^2). The time average was taken for a 10 ps interval. The open circles, squares, and diamond represent correlations $\varrho_R = \overline{R^4}/(\overline{R^2})^2 - 1$, $\varrho_S = \overline{S^4}/(\overline{S^2})^2 - 1$, and $\varrho_{RS} = \overline{R^2S^2}/(\overline{R^2})(\overline{S^2}) - 1$. The solid circles indicate $\varrho = \varrho_{RS}/(\varrho_R\varrho_S)^{1/2}$. The horizontal lines represent the unperturbed values of ϱ. Often ϱ_R, ϱ_S, and ϱ_{RS} have similar values, causing ○, □, and ◇ to be superimposed on one another.

mol^{-1} monomer,$^{-1}$ which mainly arises from the long-range van der Waals terms.

DP vs S. The time-averaged radii of gyration are plotted against DP in Figure 6. The interval for averaging varies with DP depending on the lengths of stage III$_S$. For chains with DP < 40 which do not collapse, it was the entire simulation range (200 ps).

The slope gradually decreases with increasing DP. We find the following relations for the high- and low-DP regions:

$$S = 3.15\mathrm{DP}^{1/3}, \quad \mathrm{DP} > 40 \tag{2}$$

$$= 1.80\mathrm{DP}^{1/2}, \quad \mathrm{DP} < 30 \tag{3}$$

The exponent 1/3 in eq 2 is expected from the S vs E plot since the chain collapses close to the experimental density. This exponent together with Figure 6 suggests

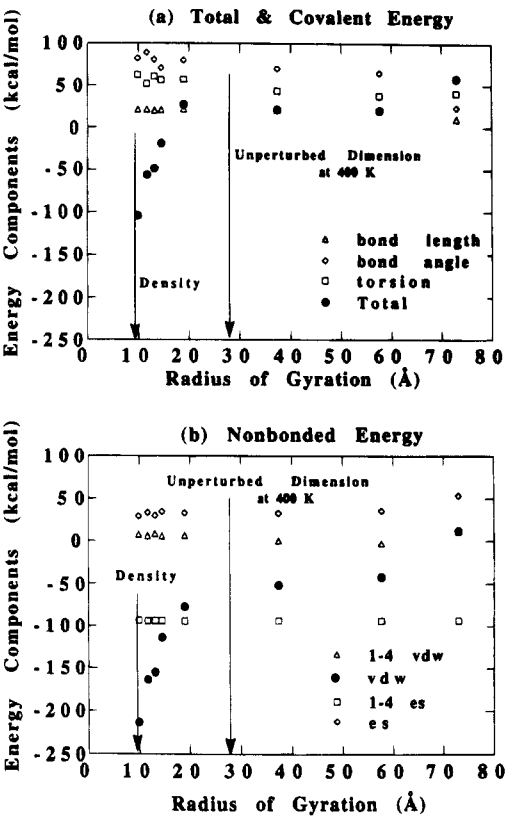

Figure 5. Potential energy and its components versus S for eight conformations selected from the MD trajectory for the 100-mer PVC chain at 600 K and then subjected to energy minimization. The symbols are (△) for bond length, (◇) for bond angle, (□) for torsion, and (●) for total energy in (a) and (△) for 1−4 van der Waals, (●) for van der Waals (rest), (□) for 1−4 electrostatic, and (◇) for electrostatic (rest) energy in (b). The vertical arrows indicate S_0 and S_{dense}, respectively.

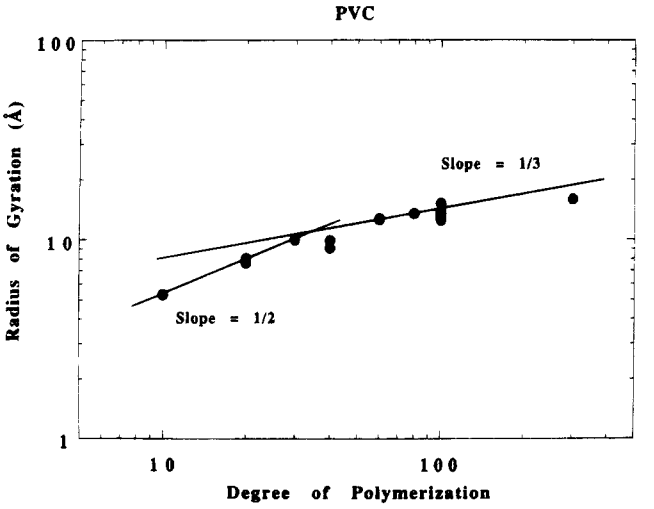

Figure 6. Time-averaged radii of gyration plotted against DP. Two lines with slopes of 1/2 and 1/3 are fitted to low- and high-DP data.

that PVC chains collapse if their DP is greater than 40. The critical length of collapse is DP = 40 for atactic PVC chains. On the other hand, the exponent 1/2 in eq 3 indicates that PVC chains are in the unperturbed state for DP < 30. This validates the Lee−Mattice assumption[34] that MD simulations of short chains give backbone torsion probabilities that can be used to construct unperturbed chains or determine the statistical weight for the rotational isomeric state model calculation.

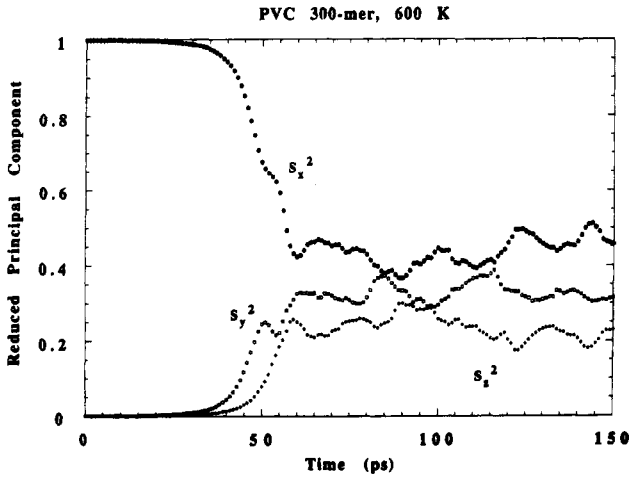

Figure 7. Trajectories of reduced principal axis components for the radius of gyration for the 300-mer at 600 K. $S_x^2 \geq S_y^2 \geq S_z^2$ are assumed.

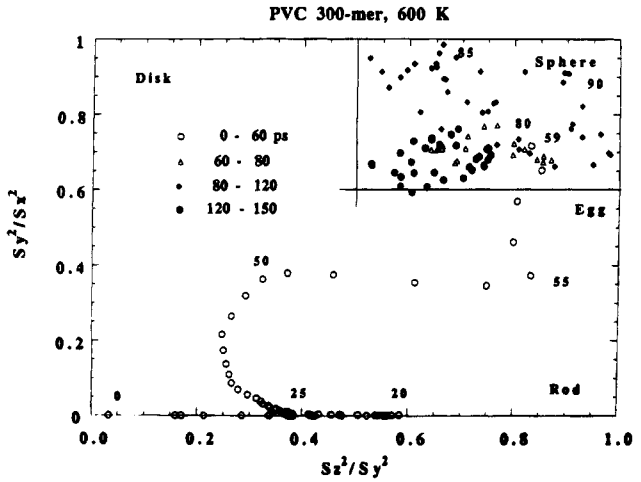

Figure 8. Trajectories of shape for the 300-mer at 600 K; (○) for 0–60 ps, (△) for 60–80 ps, (◆) for 80–120 ps, and (●) for 120–150 ps. The attached figures indicate the respective time steps.

Shape. In order to see how the shape of a chain varies during a transition from a fully extended all-*trans* conformation to a compact globule, we calculated the principal components S_x^2, S_y^2, and S_z^2 for the radius of gyration.[40] The subscripts are assigned such that $S_x^2 \geq S_y^2 \geq S_z^2$ and their sum is S^2.

Figure 7 shows trajectories of S_x^2, S_y^2, and S_z^2 reduced by S^2 for the 300-mer at 600 K. For the first 30 ps, the largest principal component, S_x^2, is dominant and close to 1. S_y^2 and S_z^2 are negligible during this period. The chain is more or less a long rod. For the next 10 ps, S_x^2 slowly decreases and S_y^2 and S_z^2 increase. The shape of the chain becomes like a sausage. Then, S_x^2 sharply decreases while S_y^2 and S_z^2 significantly increase. This lasts until the end of stage I_S or the early part of stage II_S. S_x^2 exhibits a local minimum while S_y^2 and S_z^2 have a maximum. Qualitatively similar behaviors are seen with the 100-mer at 300 and 600 K.

The three curves in Figure 7 are combined into a single one in a shape distribution plot[41] of S_z^2/S_y^2 vs S_y^2/S_x^2 in Figure 8. Different symbols represent different time intervals. The first 60 ps data points are clearly distinguished from the rest of the data. As mentioned above, this time interval corresponds to stage I_S and the beginning of stage II_S.

The plot is most instructive to understand the shape of the polymer chain during the collapse transition. For the first 25 ps, the largest principal component S_x^2 is extremely large compared to the second and third ones, S_y^2 and S_z^2, and thus $S_y^2/S_x^2 \sim 0$. The chain is getting shorter but is still rodlike. As seen in Figure 2c, S and R decrease linearly with time during this and the next 25 ps interval. During the next 25 ps, S_x^2 continues to decrease, while S_y^2 and S_z^2 increase at slightly different rates, yielding a semicircular pattern in Figure 8. S_y^2 and S_z^2 are no longer negligible. The chain is now an ellipsoid with axial ratios of 2.5:1.6:1. A horizontal array of points for the next 5 ps arise from a decrease in S_y^2 at nearly the same rate of S_x^2 while S_z^2 increases. From 55 to 60 ps S_y^2 and S_z^2 increase while S_x^2 stays constant, resulting in a vertical pattern. The chain is more spherically symmetric and the axial ratios are S_x:S_y:S_z = 1.30:1.14:1 at 60 ps.

Though R and S decrease linearly with time during the transition from the fully extended conformation to the collapsed chain, the shape of the polymer varies considerably from a thin rod to a thick sausage and to a nearly spherical ellipsoid.

Data points are in a region defined by $0.5 < S_z^2/S_y^2$ and $0.6 < S_y^2/S_x^2$ once the chain is in the collapsed state. The chain is most spherical at the time interval between 80 and 120 ps. For the conformation at 90 ps, the ratios are simultaneously just over 0.9; i.e., S_x:S_y:S_z = 1.10:1.05:1. The largest component is only 10% longer than the shortest one.

Data points corresponding to collapsed states are confined to a broader region, defined by $0.5 < S_z^2/S_y^2 < 0.9$ and $0.19 < S_y^2/S_x^2 < 0.42$ for the PVC chain of DP = 100 at 300 K. At 600 K, the 100-mer chain is more spherical than that at 300 K, as expected, but its shape fluctuation is quite large. Data points are in a region defined by $0.25 < S_z^2/S_y^2$ and $0.2 < S_y^2/S_x^2$. The ratios S_z^2/S_y^2 or S_y^2/S_x^2 individually, but not simultaneously, can be close to 1. There is no conformation whose S_y^2/S_x^2 is larger than 0.6 *and* whose S_z^2/S_y^2 is larger than 0.75.

In order to see average shapes and distribution in collapsed chains, time averages of S_x^2, S_y^2, and S_z^2, and ϱ_S for each component were calculated and listed in Table 3. For comparison purposes, the random flight values are also included.[41] As the temperature becomes higher and the chain is longer, the shape becomes more spherically symmetric. The higher the temperature and the shorter the chain, the broader the distribution. The distributions for 300-mer PVC are limited to ±30% from the mean.

The ratios and distributions of the principal components and the shape distribution for collapsed states are very different from those of random flight chains. As listed in Table 3, the ratios of the principal components for random flight chains are much larger than those of any collapsed chains. Distributions for the principal components of random flight chains are skewed and long tails exist at the larger value of $S_u^2/\mathrm{Av}(S_u^2)$ ($u = x, y, z$).[41] Their most probable peak positions are less than their mean values, and the larger component has a peak at a smaller value of the relative value of $S_u^2/\mathrm{Av}(S_u^2)$.

Table 3. Ratios for the Principal Components of the Radius of Gyration of Collapsed Chains

polymer	S_x^2	S_y^2	S_z^2	ϱ_{S_x}	ϱ_{S_y}	ϱ_{S_z}
PVC 100-mers at 300 K	5.5	1.9	1	0.009	0.014	0.021
PVC 100-mers at 600 K	3.9	1.7	1	0.054	0.051	0.039
PVC 300-mers at 600 K	1.8	1.4	1	0.010	0.004	0.018
random flight chain (100 bonds)	11.6	2.7	1			

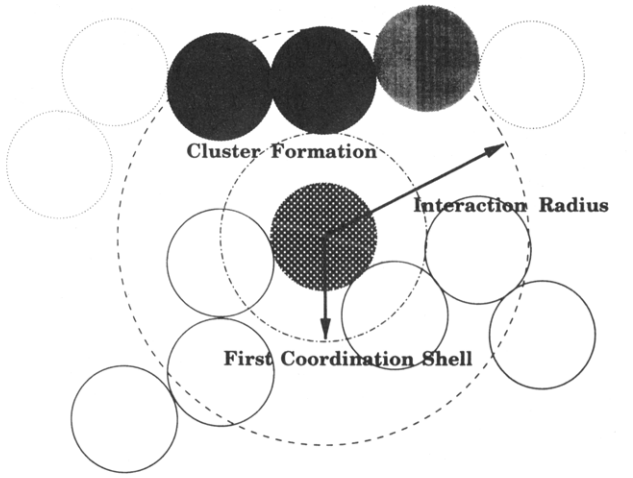

Figure 9. A schematic representation of cluster formation in a polymer chain. A reference monomer and its three nearest neighbors along the chain contour are depicted in the bottom portion of the figure. Another subchain of six monomers is displayed at the top. The gray scale shows the relative strength of interactions of these six monomers with the reference monomer. The chain and dashed circles indicate the first coordination shell and interaction radius, respectively.

Monomers in the Clusters. When a chain is in a loose coil state, monomer–monomer contacts are infrequent, since an average monomer density per unit volume is low. If monomer interactions are attractive, the polymer domain becomes smaller and the monomer density increases. This reduction in dimensions causes more and more attractive interactions and the chain size must decrease more and more. However, since each monomer has a finite volume due to the van der Waals radii of individual atoms, the long-range attractive interactions cease at a short distance between monomers. For PVC chains, interaction between monomers becomes repulsive at less than 4 Å. The dimension of collapsed chains is determined by a balance between attractive and repulsive interactions. Thus, we first count how many monomers are interacting with a reference monomer in terms of a cluster.

A cluster may be defined with the aid of Figure 9. A reference monomer forms a cluster with other monomers which are separated more than 5 monomer units along the chain contour, if they are within a certain distance (interaction radius, R_i), i.e., 8 Å. The number of monomers separated along the contour is arbitrary. Yet, we chose 5 monomers apart because an 8 Å radius from one carbon atom in a reference monomer extends up to the third nearest-neighbor monomers in a fully extended PVC chain.

The main chain atoms are the methylene and methine carbons in a PVC chain. We regard them as representatives of each monomer. If any of the carbon–carbon distances is shorter than R_i, monomers to which the carbons belong are considered to form a cluster. Distant monomers often partially lie within R_i as shown in a different gray scale in Figure 9. Such monomers contribute to the number of monomers 1/4, 1/2, or 3/4 depending on the number of carbon–carbon pairs less than 8 Å.

The number of monomers in the clusters are plotted against the simulation time for the 100-mer at 300 K in Figure 10. The number of monomers in the clusters remain zero until 35 ps, indicating that no long-range clustering occurs during this time period (I_m). Between 40 and 60 ps, it sharply increases from 10 to 62% (II_m)

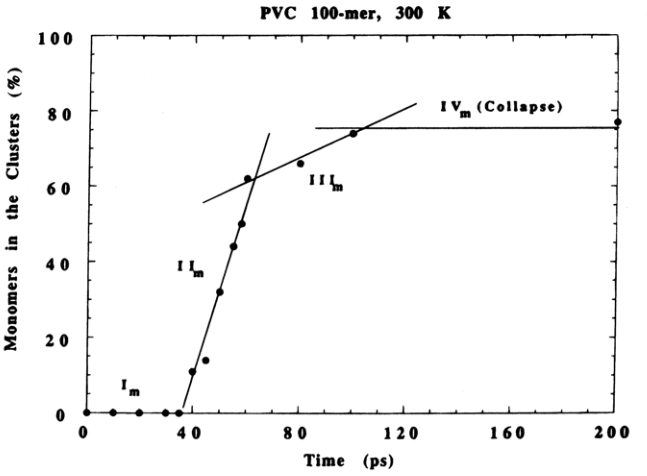

Figure 10. Percent of the monomers in the clusters of 8 Å radius plotted against the simulation time for 100-mer PVC at 300 K. The straight lines are fitted to data points in each region. Stages I_m, II_m, III_m, and IV_m (collapse) are discussed in the text.

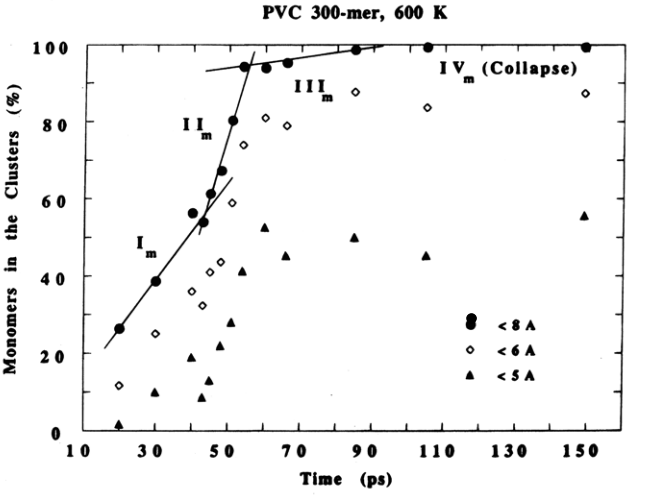

Figure 11. Percent of the monomers in the clusters of 5 (▲), 6 (◇), and 8 (●) Å radii plotted against the simulation time for 300-mer PVC at 600 K. The straight lines are fitted to data points of 8 Å radius in each region. Stages I_m, II_m, III_m, and IV_m are discussed in the text.

and continues to grow gradually to 75% until around 120 ps (III_m). After that, it remains around 75% (IV_m). Similarly, in Figure 11 for the 300-mer chain the number of monomers in the clusters linearly increases for the first 40 ps (I_m). For the next 15 ps, it sharply increases to about 95% (II_m), and then it continues to grow, though slowly, until 85 ps (III_m). Almost all monomers are in the clusters by 85 ps and remain so for the duration of the simulation (IV_m).

For the process from a fully extended conformation to a collapsed coil, the monomer clustering here exhibits three stages instead of two found in the trajectories of S. The first stage (I_m) is a slow growth of clusters or the formation of clusters, which are nuclei of further clustering. In the second stage (II_m), nearly the entire chain becomes a single large cluster with some monomers left out from it. In the final stage (III_m), monomer pairs which are in the molecular cluster but far away from each other come into contact, and the chain becomes compact.

S seems to be insensitive to the beginning of clustering, but R exhibits a small shoulder at around that time. In both 100-mer and 300-mer chains, the transition of S from I_S to II_S corresponds to the middle of stage II_m.

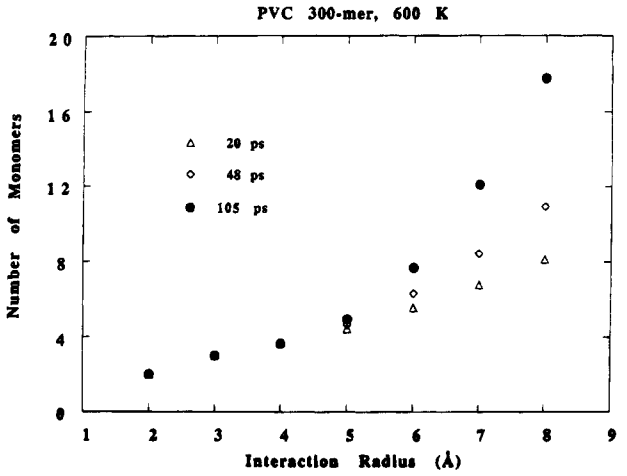

Figure 12. Number of monomers within interaction radii for 300-mer PVC at 600 K. The triangles, diamonds, and solid circles are for 20, 48 and 105 ps time steps, respectively.

Figure 11 also contains percentages of monomers within 5 and 6 Å from any monomers separated more than 5 monomers along the contour. For the collapse time domain, almost all monomers have distant monomers within 8 Å, and more than 80% of monomers do within 6 Å. A monomeric PVC unit may be approximated by a sphere of radius 2.6 Å whose density is the same as the bulk one. Figure 11 shows half of the monomers have distant monomers along the contour within the first coordination shell of 5.2 Å (chain circle in Figure 9). The other half has only the first to fourth nearest monomers along the contour there.

Figure 12 displays the average number of monomers at 20, 48, and 105 ps within a sphere of R_i varying from 2 to 8 Å. There is no room for nonbonded monomers in a sphere of less than 4 Å radius, which is close to one and a half of the PVC monomer radius. Covalently connected monomers and one carbon atom in the second nearest-neighbor monomers fill the sphere of 4 Å. Even though at 20 ps the chain has a much larger dimension than the unperturbed one and at 105 ps it is in the most compact state, the first coordination shell (~5 Å) is filled with a very similar number of monomers: It is occupied by 3.4 monomers at 20 ps and by 3.9 monomers at 105 ps. However, as displayed in Figure 11, at 20 ps few monomers have neighbors within 5 Å from the contour more than 5 monomers away. The first coordination shell is filled with only the nearest few monomers along the contour. On the other hand, at 105 ps half of the monomers have at least one distant monomer in the shell. At distances larger than the first coordination shell, an appreciable difference appears in the number of monomers between extended (20 ps) and compact (105 ps) conformations.

Figure 13 demonstrates that the initial clustering is local and a sharp increase in a monomer fraction is due to long-range clusterings. Here, the monomers are classified into three groups depending on the distance along the chain contour from a particular monomer. The first group consists of monomers which are 2–4 units away along the contour. These are excluded when the clustering is considered above. Since the sum of the groups up to a separation along the contour of 20 monomers is virtually unaffected by the collapse, one can infer that such a chain would have no motive to collapse, which is consistent with our finding in Figure 6. The second and third groups are 5–50 and more than 50 units away from the reference monomer, respectively.

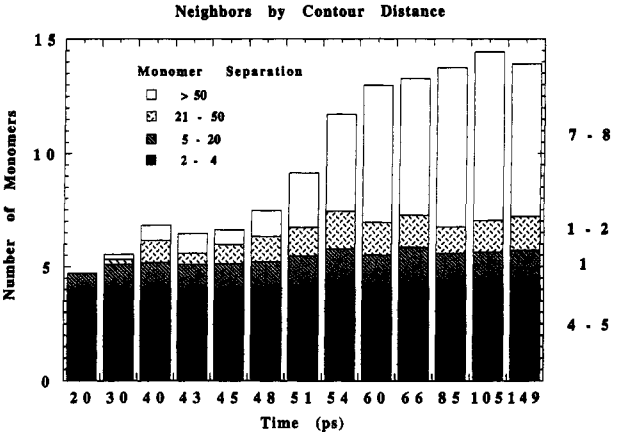

Figure 13. Number of monomers in the clusters of an 8 Å radius plotted against the simulation time for 300-mer PVC at 600 K. The gray scale varies from black to white with the contour distance from the reference monomer to the monomers in the cluster. The figures on the right-hand side represent the average neighbors from respective contours in the collapse state.

The number of monomers in a sphere radius of 8 Å is calculated for each monomer at a certain time step, and then it is averaged over all the monomers.

In the all-*trans* conformation of a PVC chain, which is our initial structure for the simulations, only the first to third monomers along the contour are within an 8 Å radius from the reference one. Therefore, each monomer is always surrounded by 4 monomers in the first group. In fact, this number remains constant for the first 60 ps during which the polymer dimension dramatically reduces. After that, the neighboring monomers from this group increase very gradually to 4.5 monomers. This means 1 of 4 carbons in the fourth monomers in either side from the reference is within an 8 Å radius after 60 ps.

The number of neighboring monomers from the second group is zero at the beginning as mentioned above. It starts quickly increasing by the first 30 ps due to the clustering of monomers within 5–20 units away. Then, monomers between 21 and 50 monomers away come into the 8 Å radius. The number of neighboring monomers from the second group increases gradually to about 2 by 50 ps and tends to saturate at around 2–2.5 monomers after 50 ps. The long-range clustering with monomers more than 50 monomers away along the contour starts at around 30 ps, after the initial cluster formation occurs with monomers between 5 and 20 units away. It gradually increases until the chain becomes much smaller than the unperturbed dimension. For the first 45 ps, the number of neighboring monomers from the third group is one or less. While S decreases more gradually than the first 45 ps, the number of neighboring monomers from this group significantly increases for the next 10–15 ps. After 60 ps, it saturates to 6–9 neighbors which are more than 50 monomers away along the contour.

Though the chain becomes compact, the monomer environment is inhomogeneous in the chain domain. Figure 14 displays the distribution of the number of neighboring monomers within 8 Å and separated at least 5 monomers along the contour for collapse conformations at 85, 105, and 149 ps. The distribution has a fairly broad peak from 3 to 13, centered at 9.6 monomers. About 2–3% of monomers have no neighbors except those less than 5 monomers along the contour.

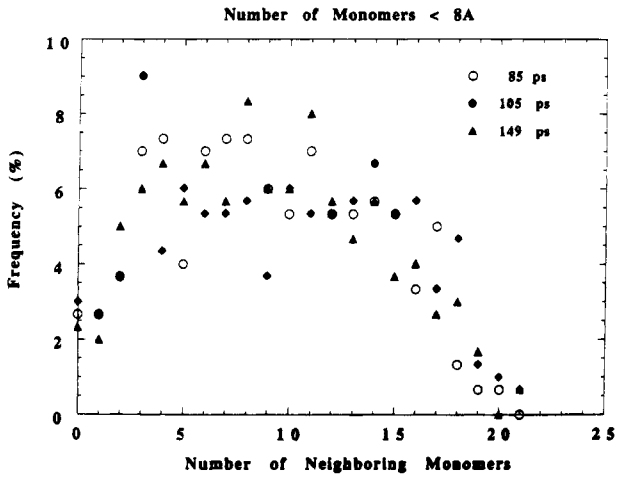

Figure 14. Distribution of the number of neighboring monomers within 8 Å for collapse conformations at 85 (○), 105 (◆), and 149 (▲) ps for 300-mer PVC at 600 K.

All monomers have less than 21.5 neighbors within 8 Å, which is estimated from the experimental density. Many could accommodate ~10 more monomers within an interaction radius of 8 Å. The chain in the collapsed state attained in the simulation at 600 K contains a large amount of vacancy.

Further, the number of neighbors significantly varies along the contour. Dense and scarce neighbor domains alternatively appear along the chain contour. The size of each domain varies from a few monomers to 20–40 monomers. These domains are unsteady and change with time along the contour. Therefore, the monomers retain the mobility in the collapsed state attained in the simulation at 600 K.

Distance Plot. Now we study the collapse mechanism by the distance plot. Before going into the analysis of PVC chains, it is preferable to present some basic patterns appearing in the plot.

In the distance plot with the monomer serial number as both axes, we mark a dot at (i, j) when the two monomers, i and j, come closer than a certain distance, i.e., 8 Å. A single isolated mark means that the corresponding monomers are in contact. Since a polymer chain is covalently bonded, near-neighbors along the chain contour always exist at close distances. These appear along the diagonal line from the left bottom to the right top in the distance plot. A parallel pattern to the diagonal line indicates that two portions of the chain are in parallel in a sense that the segment index increases for both portions. If the pattern is close to the diagonal line, it is necessarily a helix, for example, the α helix in poly(amino acids). The distance between the diagonal line and a particular pattern corresponds to the contour length of a dangling loop between two portions for the pattern.

If a pattern is perpendicular to the covalent diagonal line, it is an antiparallel alignment including a hairpin folding whose loop length depends on the length from the diagonal line. For immediate foldings, the pattern starts from the diagonal line such as a β turn in poly(amino acids). A lamella exhibits a rectangle with two pairs of sides parallel and perpendicular to the diagonal line.

Figure 15 displays distance plots for the 300-mer PVC chain at 40 (a), 45 (b), 54 (c), and 105 (d) ps. The first three plots correspond to time steps when the increment for the percentages of monomers in the clusters significantly increases, and the chain is the most compact at 105 ps.

As seen in Figures 2c and 15a, the last half of the chain has folded by 40 ps, but the first half has not. The distance plot shows that one end (300th-mer side) forms clusters with six other parts of the chain. Hairpin foldings appear along the diagonal line and are close to the end, though they are more than 8 Å away from each other. There is an inner triangle region where no monomer forms any cluster.

By 45 ps (b), the middle section forms several clusters, but some previously existing ones disappear, particularly around the end and near the diagonal line. Two clusters developed in the first 100-mer region, but still the first half is away from the second one.

At 54 ps, nearly 95% of monomers are involved in the clustering, as seen in Figures 11 and 15c. No clustering is found at a portion between the 130th and 145th monomers. The last 60 monomers actively interact with many other portions of the chain. Yet, we find again a large triangle region without any point. It is noted that a hairpin loop at the first 20 monomers almost disappears. This is very different from the aggregation mechanism at the ends in the irreversible collapse simulation.[32]

The most compact conformation at 105 ps (d) has clustering points all over. However, their distribution is inhomogeneous. Quite a few monomers do not have neighbors from the contour less than 100 monomers away; however, almost all have close neighbors from the contour more than 150 but less than 250 monomers away. The largest loop is formed between the 20–30th and 295–300th monomers. A horseshoe pattern is one noteworthy feature of this figure. It originates from a loose self-entanglement appearing between the 30–65th and 90–130th monomers, whose snapshot is shown in the lower triangle region. Such a structure never appears until a chain is close to or in a collapsed region. The patterns at 40, 45, and 54 ps arise from mostly parallel or antiparallel arrangements of chain portions, and chains have no entanglements.

The number of self-entanglements may be evaluated as the ratio of the total number of contacts N_c at large scales to the number of entanglement degree of polymerization N_e.[19] Since the counting of N_c is ambiguous, we assume that N_c for collapsed chains is proportional to the ratio of the number of carbon–carbon pairs within a given R_i to that of the unperturbed one and N_c of the unperturbed chain, which is of the order of $N^{1/2}$. N_e is known to be around 70 for a melt of PVC.[42] Further, our unperturbed state is assumed to be where S becomes equal to S_0. Using this value and varying R_i from 5 to 8 Å, we have 1–2.4 self-entanglements in a collapsed PVC chain. The self-entanglement is too low (~0.25) to occur at the unperturbed state. The chain must become more compact than the unperturbed dimension. The self-entanglement may appear only in the second stage (II_S) of collapsing.

Torsion Distribution. In our above analysis, we found that the chains in collapsed states have much smaller dimensions than at the unperturbed state due to long-range van der Waals attractive interactions. Also, the torsion energy increases about 10% compared to the unperturbed state. Now we may ask whether any new torsion states are developed or only the distribution of *trans* and *gauche* states is shifted in the collapsed state.

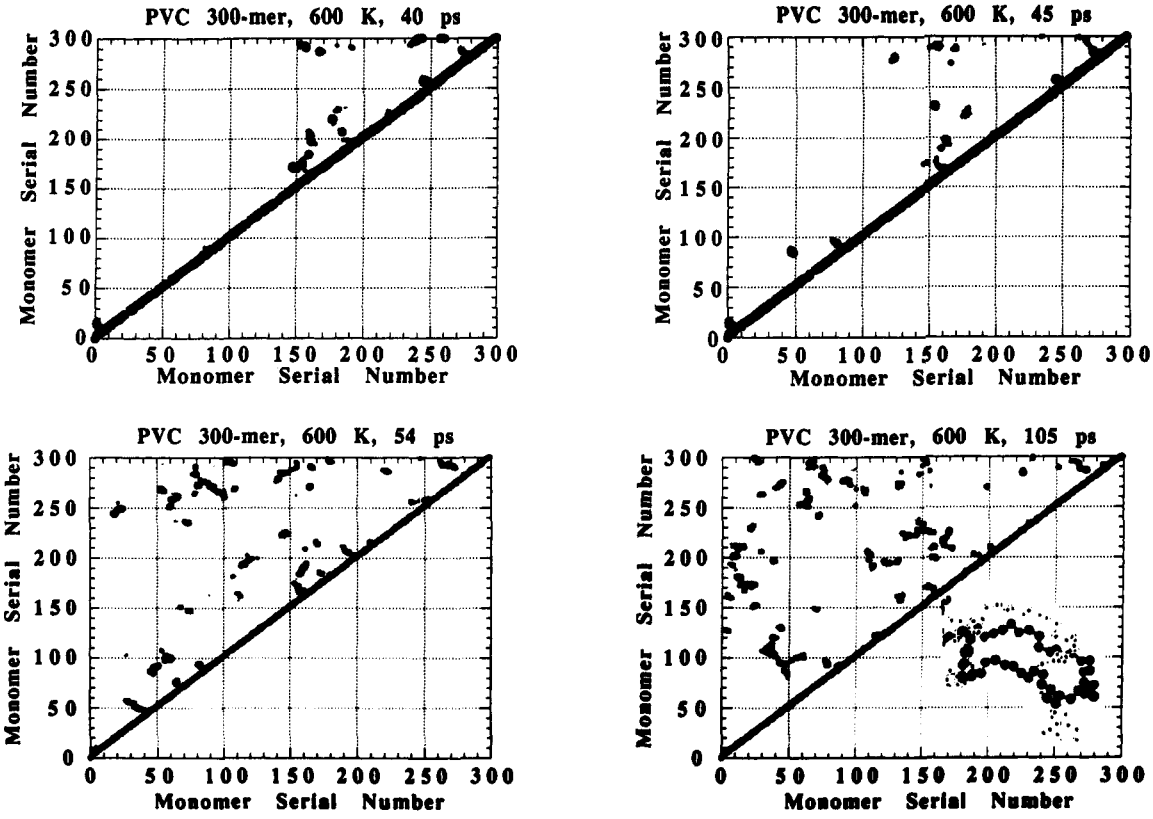

Figure 15. Distance plots for conformations at (a) 40, (b) 45, (c) 54, and (d) 105 ps of 300-mer PVC chain at 600 K. The dots indicate that a pair of monomers are within 8 Å. The ball–stick model drawn in (d) shows a self-entanglement corresponding to the horseshoe pattern.

Table 4. Characteristics of Collapsing Stages

property	I_m	II_m	III_m	IV_m (collapsed state)
S stage	I_S	$I_S \rightarrow II_S$	II_S	III_S
S	$>S_0$	$S_0 \rightarrow (1.6-1.9)S_{dense}$	slow decreasing	$\sim(1.2-1.4)S_{dense}$
R	$>R_0$	$<R_0$; marked minimum	$<R_0$; large fluctuation	$<R_0$; large fluctuation
dS/dt	constant $\ll 0$	increasing	constant < 0	~ 0
dR/dt	constant $\ll 0$	$\pm$constant	chaotic	chaotic
R^2/S^2	decreases	distinctive minimum	large fluctuation	large fluctuation
ϱ	~ 1	$\rightarrow 0$	very large fluctuation	very large fluctuation
total potential energy	slight decrease	slight decrease	sharp decrease	fluctuation
long-range vdW energy	slight decrease	slight decrease	sharp decrease	fluctuation
electrostatic energy	nearly constant	nearly constant	nearly constant	nearly constant
S_y^2/S_x^2 (DP = 300)	<0.02	<0.7	>0.6	>0.6
S_z^2/S_y^2 (DP = 300)	<0.6	0.25–0.85	>0.5	>0.5
trans content	sharp decrease	slight decrease	nearly constant	nearly constant
clustering monomers	appearing	sharp increase	slight increase	constant
self-entanglement	none	none	appearing	appearing

We examined trajectories of several bonds whether or not any new torsional states developed in collapse states. Some bonds fluctuate between 50 and 180° rather uniformly. However, most bonds remain around the normal three states, *trans* and gauche$^{\pm}$. Therefore, we assigned torsion angles between ±180 and ±120° to the *trans* state, between +45 and +120° to the *gauche* +60° state, and between −120 and −45° to the *gauche* −60° state. Torsion values have never fallen in the range between ±45° during the duration of the simulation.

Figure 16 displays the content of *trans* and *gauche* states for the 100-mer at 300 K and the 300-mer at 600 K at several time steps. All bonds are in the *trans* state at the beginning of the simulation, and 15–35% of them transform into the *gauche* states within 50 or 60 ps after stage I_S is completed. After that, the torsion distribution seems to reach an asymptote soon. The 100-mer chain has 75% of *trans* even after the chain collapses, while the 300-mer chain has around 60%. These values are only 4–13% lower than those of the unperturbed chain.[34,38,43] The fraction of the *trans* state is less in the 300-mer chain than in the 100-mer chain, because the shorter chain is, in a relative sense, more expanded than the longer one as α_S in Table 2 shows.

The distribution of individual torsion angles is quite different from those expected from the average values over the entire chain. The percentage of the time an individual bond spends in the *trans* state varies greatly from 7 to 100%. In collapsed chains, individual bonds tend to stay in a single torsion state.

There are one 20 and one 23 *trans* sequences in the 100-mer, and the rest are less than 9 bonds long. The 300-mer has shorter *trans* sequences: the maximum length is only 13 bonds. A single *trans* bond has the highest percentage in the 300-mer while in the 100-mer the *trans–trans* bonds are slightly richer than an isolated *trans* bond. *Gauche* bonds are predominantly single.

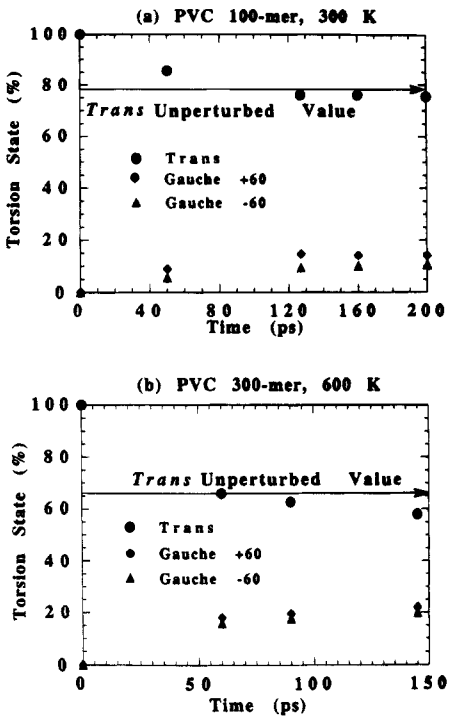

Figure 16. Content of torsion states for (a) the 100-mer at 300 K and (b) the 300-mer at 600 K. The horizontal arrows indicate the content of the *trans* state in the unperturbed chains.

Concluding Remarks

We have simulated atomistic PVC chains in vacuum and extensively analyzed molecular dimensions, shape, monomer contacts, and torsion angles. An isolated PVC chain quickly folds into a compact collapsed state for DP > 40 and remains unperturbed for DP < 30. This result is consistent with an indication[1] obtained from the original Flory equation[44] containing only the binary cluster integral. As the chain becomes compact, ternary contacts as well as binary become frequent and affect the chain dimension. However, as the perturbation theory predicts,[45-47] the chain dimension may be a function of the effective binary-cluster integral that is a linear combination of binary- and ternary-cluster terms.[48] In other words, the effect of ternary collisions on chain dimensions is irrevelant. This may be the reason that the binary-cluster approximation qualitatively predicts the chain length dependence of collapsing.

Based on our analysis, we summarized the main characteristic features of various properties in the individual collapsing stages in Table 4. Each stage may be described as follows: Initially, a fully extended chain locally shrinks, bends, and forms clusters such as loops, turns, and spirals (one-turn helix) mainly among close neighbors along the contour. The fraction of the *trans* states decreases considerably. This is the first stage of collapsing where both R and S sharply decrease with time and become less than the unperturbed values. The shape of the chain changes from a thin wire to a sausage.[19]

Stage II_m corresponds to the transition from a sharp to a gradual decrease in S. During this stage, distant monomers along the contour start coming within an interaction radius of each monomer. Yet, the clusters are of the parallel or antiparallel type. The correlation between R and S is lost and the chain radius thickens. R exhibits a distinctive minimum.

The third stage (III_m) corresponds to the later part of II_S, being characterized by an appearance of self-entanglements. Because of the long-range van der Waals forces, S gradually becomes smaller. Clusters attract each other and develop more complex clusters with distant monomers including self-entanglements. The shape of the chain is close to a slightly elongated ellipsoid which is more spherical than the unperturbed one (random flight chain). The number of contacts is one factor but the shape of the chain is another to form self-entanglements since entanglements are of a 3-D nature.

The two-stage process appearing in S is consistent with recent light scattering experiments[12] and theoretical predictions.[19,22] On the other hand, our analysis of monomer clustering shows a three-stage process to collapse. The microscopic process is more complex than the global one.

In the collapsed state (IV_m), S remains nearly constant while R fluctuates greatly. The nearest few monomers tend to stick together, yielding a dense core of one and a half monomer radius. Beyond the core each monomer has roughly 60–70% of the neighbors calculated from the bulk density. The monomers retain a greater mobility in the collapsed state than in the amorphous state. In this connection, it is pointed out that a recent experiment by Chu et al. found[49] that the collapsed globule contains a great amount of solvent.

Since each PVC monomer has about 10 distant monomers with an energy of around 1.5 kcal mol^{-1} $monomer^{-1}$ in a collapsed state, an interaction energy for a pair of monomers is only 0.15 kcal mol^{-1}. This is nearly one-hundredth of a typical hydrogen-bonding energy and one-quarter of the kinetic energy at room temperature. Though small, the attractive interaction is crucial. However, energetics alone does not dictate the collapsing. There are a number of interaction pairs and a number of combinations of forming pairs in a long flexible chain. Such entropic nature plays a significant role in collapsing a long chain.[25] Short chains have less entropy due to a limited number of pairs and do not collapse. If a chain is stiff, a strong interaction is needed to compensate a small entropic contribution or the chain must be long for the chain to collapse.

In the precent work, the chain collapsing time is 60–120 ps and much shorter than the experimental 100 s.[49] The difference arises partly from the viscosity and partly from the chain size. Since the latter accounts for around 10^5, the viscosity effect must be of order 10^7. When a chain is a loose coil at the initial stage, the correction is due to the solvent viscosity; however, when the chain becomes compact, the viscosity is no longer the solvent viscosity but may have a contribution of surrounding monomers. A single correction factor yields erroneous results. Thus, we avoid any comparison involving time constants.

Acknowledgment. G.T. thanks Drs. R. G. Wissinger and L. Soby for their interest and encouragement in the early stage of this work. This work was supported by the BFGoodrich Co.

References and Notes

(1) Stockmayer, W. H. *Makromol. Chem.* **1960**, *35*, 54.
(2) Yamakawa, H. *Modern Theory of Polymer Solutions*; Harper and Row: New York, 1971.
(3) Cuniberti, C.; Bianchi, U. *Polymer* **1974**, *15*, 346.
(4) Slagowski, E.; Tsai, B.; McIntyre, D. *Macromolecules* **1976**, *9*, 687.

(5) Sun, S.; Nishio, I.; Swislow, G.; Tanaka, T. *J. Chem. Phys.* **1980**, *73*, 5971.
(6) Miyaki, Y.; Fujita, H. *Polym. J.* **1981**, *13*, 749.
(7) Persynski, R.; Adam, M.; Delsanti, M. *J. Phys.* **1984**, *45*, 1765.
(8) Vidakovic, P.; Rondelez, F. *Macromolecules* **1984**, *17*, 418.
(9) Park, I. H.; Wang, Q.-W.; Chu, B. *Macromolecules* **1987**, *20*, 1965.
(10) Chu, B.; Park, I. H.; Wang, Q.-W.; Wu, C. *Macromolecules* **1987**, *20*, 2833.
(11) Park, I. H.; Fetters, L.; Chu, B. *Macromolecules* **1988**, *21*, 1178.
(12) Yu, J.; Wang, Z.-L.; Chu, B. *Macromolecules* **1992**, *25*, 1618.
(13) Ptitsyn, O. B.; Kron, A. K.; Eizner, Yu. E. *J. Polym. Sci., Part C* **1968**, *16*, 3509.
(14) Lifshitz, I. M.; Grosberg, A. Y.; Khokhlov, A. R. *Rev. Mod. Phys.* **1978**, *50*, 683.
(15) Sanchez, I. *Macromolecules* **1978**, *12*, 980.
(16) Post, C. B.; Zimm, B. H. *Biopolymers* **1979**, *18*, 1487.
(17) Muthukumar, M. *J. Chem. Phys.* **1984**, *81*, 6272.
(18) Di Marzio, E. A. *Macromolecules* **1984**, *17*, 969.
(19) de Gennes, P.-G. *J. Phys. Lett.* **1985**, *46*, L-639.
(20) Allegra, G.; Ganazzoli, F. *J. Chem. Phys.* **1985**, *83*, 397.
(21) Birshtein, T. M.; Pryamitsyn, V. A. *Vysokomol. Soedin.* **1987**, *29A*, 1858.
(22) Grosberg, A. Yu.; Nechaev, S. K.; Shakhnovich, E. I. *J. Phys.* **1988**, *49*, 2095.
(23) Grosberg, A. Yu.; Kuznetsov, D. V. *Macromolecules* **1992**, *25*, 1970.
(24) Grosberg, A. Yu.; Kuznetsov, D. V. *Macromolecules* **1992**, *25*, 1980.
(25) Grosberg, A. Yu.; Kuznetsov, D. V. *Macromolecules* **1993**, *26*, 4249.
(26) McCrackin, F. L.; Mazur, J.; Guttman, C. L. *Macromolecules* **1968**, *1*, 859.
(27) Webman, I.; Lebowitz, J. L.; Kalos, M. H. *Macromolecules* **1981**, *14*, 1495.
(28) Kremer, K.; Baumgärtener, A.; Binder, K. *J. Phys. A: Gen. Math.* **1981**, *15*, 2879.
(29) Kolinski, A.; Skolnick, J.; Yaris, R. *J. Chem. Phys.* **1986**, *85*, 3585.
(30) Kolinski, A.; Skolnick, J.; Yaris, R. *Biopolymers* **1987**, *26*, 937.
(31) Karasawa, N.; Goddard, A. A., III. *J. Phys. Chem.* **1988**, *92*, 5828.
(32) Ostrovsky, B.; Bar-Yam, Y. *Comput. Polym. Sci.* **1993**, *3*, 9.
(33) Kavassalis, T. A.; Sundararajan, P. R. *Macromolecules* **1993**, *26*, 4144.
(34) Lee, K.-J.; Mattice, W. L. *Comput. Polym. Sci.* **1991**, *1*, 213.
(35) Clark, M.; Cramer, R. D., III; van Opdenbosch, N. *J. Comput. Chem.* **1989**, *10*, 982.
(36) Berthod, H.; Pullman, A. *J. Chem. Phys.* **1965**, *62*, 942.
(37) Ludovice, P. J.; Suter, U. W. In *Computational Modeling of Polymers*; Bicerano, J., Ed.; Marcel Dekker: New York, 1992; pp 401–435.
(38) Smith, G. D.; Jaffe, R. L.; Yoon, D. Y. *Macromolecules* **1993**, *26*, 298.
(39) Mattice, W. L.; Sienicki, K. *J. Chem. Phys.* **1989**, *90*, 1956.
(40) Šolc, K.; Stockmayer, W. H. *J. Chem. Phys.* **1971**, *54*, 2756.
(41) Šolc, K. *Macromolecules* **1973**, *6*, 378.
(42) van Krevelen, D. W. *Properties of Polymers*, 3rd ed.; Elsevier: Amsterdam, 1990.
(43) Mark, J. E. *J. Chem. Phys.* **1972**, *69*, 451.
(44) Flory, P. J. *Principles of Polymer Chemistry*, 5th ed.; Cornell University Press: Ithaca, NY, 1966.
(45) Yamakawa, H. *J. Chem. Phys.* **1966**, *45*, 2606.
(46) Cherayil, B. J.; Douglas, J. F.; Freed, K. F. *J. Chem. Phys.* **1985**, *83*, 5293.
(47) Norisuye, T.; Nakamura, Y. *Polymer* **1993**, *34*, 1440.
(48) Yamakawa, H. *Macromolecules* **1993**, *26*, 5061.
(49) Chu, B.; Ying, Q.; Grosberg, A. Y. *Macromolecules*, submitted.

MA941106F